atmosphere

MDPI

Article

Giant *Aufeis* in the Pangong Tso Basin: Inventory of a Neglected Cryospheric Component in Eastern Ladakh and Western Tibet

Tobias Schmitt [1], Dagmar Brombierstäudl [1], Susanne Schmidt [1] and Marcus Nüsser [1,2,*]

[1] Department of Geography, South Asia Institute (SAI), Heidelberg University, 69115 Heidelberg, Germany; tobias.schmitt01@stud.uni-heidelberg.de (T.S.); brombierstaeudl@uni-heidelberg.de (D.B.); s.schmidt@uni-heidelberg.de (S.S.)
[2] Heidelberg Center for the Environment (HCE), Heidelberg University, 69120 Heidelberg, Germany
* Correspondence: marcus.nuesser@uni-heidelberg.de; Tel.: +49-6221-5415241

Abstract: Cryosphere studies in High Mountain Asia (HMA) typically focus on glaciers, seasonal snow cover, and permafrost. As an additional and mostly overlooked cryosphere component, *aufeis* occurs frequently in cold-arid regions and covers extensive areas of the Trans-Himalaya and Tibetan Plateau. This largely neglected cryosphere component generally forms in winter from repeated freezing of seepage or overflow. In this article, the occurrence of *aufeis* fields in the endorheic Pangong Tso Basin (PTB), with a total area of 31,000 km^2, is inventoried and examined. Based on a semi-automatic remote sensing approach using Sentinel-2 imagery, about 1000 *aufeis* fields were detected in the spring of 2019, covering a total area of approximately 86 km^2 and with an average individual size of 0.08 km^2, while the largest field covered an area of 14.8 km^2. A striking contrast between the northern and southern portions of the PTB characterized the spatial distribution of large *aufeis* fields. All large (>0.5 km^2) and 13 persisting *aufeis* fields were located along broad valleys in the northern portion. Furthermore, a multi-temporal comparison between 1994 and 2023 shows that the number of remaining *aufeis* fields in autumn varied between 8 and 29, with a maximum in 2019. Their total area ranged between about 0.3 km^2 in 1994 and 2023 to about 1.2 km^2 in 2015 and 2019. This study complements recent *aufeis* inventories from the Trans-Himalayan region of Ladakh and closes the gap to the Tibetan Plateau.

Keywords: *aufeis*; cryosphere; permafrost; remote sensing; Sentinel-2; High Mountain Asia

check for updates

Citation: Schmitt, T.; Brombierstäudl, D.; Schmidt, S.; Nüsser, M. Giant *Aufeis* in the Pangong Tso Basin: Inventory of a Neglected Cryospheric Component in Eastern Ladakh and Western Tibet. *Atmosphere* **2024**, *15*, 263. https://doi.org/10.3390/atmos15030263

Academic Editors: Ruiqiang Bai, Jiwei Wang and Xiao Jin

Received: 30 December 2023
Revised: 15 February 2024
Accepted: 17 February 2024
Published: 22 February 2024

Copyright: © 2024 by the authors. Licensee MDPI, Basel, Switzerland. This article is an open access article distributed under the terms and conditions of the Creative Commons Attribution (CC BY) license (https://creativecommons.org/licenses/by/4.0/).

1. Introduction

A decline of the cryosphere due to climate change can be observed in all high mountain regions [1]. In the long run, this trend will adversely affect water availability, especially in regions where cryospheric meltwater plays a significant role in the hydrological system [2–5]. This will pose increasing risks for local communities [6–9]. In contrast to the mass loss of glaciers [10–12], the depletion of snow cover [13,14], and the degradation of permafrost [15,16], the importance of a largely neglected cryospheric component, *aufeis*, is still at an exploratory stage. Its role and traditional use as an adaptation strategy against seasonal water scarcity have been reflected in several studies [17–20]. *Aufeis*, also known as "icing", "naled", or "taryn", refers to layered, surficial ice formed seasonally by repeated freezing of meltwater, ground water, or spring water on already frozen surfaces [21]. Frequent freeze–thawing cycles in permafrost areas are presumably responsible for its formation [22–25]. It is often formed in close proximity to rivers, streams, or springs, where water repeatedly emerges through frozen layers and refreezes on the surface. Due to this process, *aufeis* can accumulate into compact bodies several meters thick and of varying sizes. Under optimal conditions, it can even persist in places throughout the year [21,26,27]. A variety of factors contribute to the formation of *aufeis*. These include surface and groundwater dynamics, topographical settings, climatic conditions, seasonal snow cover, geological and soil conditions, and the presence of permafrost [28].

In contrast to studies in permafrost regions of Siberia and Alaska [21,24,28–30], long-term observations of *aufeis* distribution in High Mountain Asia (HMA) are still rare [31–34], although some researchers have already described the occurrence of *aufeis* in the Pangong Tso Basin (PTB) and neighboring regions since the mid-19th century [35–37]. Original quotations illustrate the historical evidence of *aufeis* in PTB. Strachey [35] (54) described "the occurrence of certain permanent beds of frozen snow" at "two or three places of the Changtang in the middle of summer. The Tibetans call these snowfields Dar, and assert them to be permanent, and constant from year to year in the same places. The largest were in a wide sunny valley, among low snowless mountains; and all of them in the beds of rivulets where most flat and marshy; the snow always hard frozen". The same ice fields were described by de Terra [36] (30f), who highlighted that the same "field was observed in 1848 by Strachey, whose description made it equally thick but 84 years in an open valley seems to argue against climatic oscillations of such magnitude as might otherwise be inferred from the changes of lake levels in the neighborhood", suggesting multiple year perseverance or seasonality [36]. This article presents the first detailed inventory of *aufeis* distribution in the endorheic Pangong Tso Basin using Sentinel-2 imagery. It complements recent *aufeis* inventories from the Trans-Himalayan region of Ladakh [31,32] and closes the gap to the Tibetan Plateau. It also analyzes the occurrence of giant *aufeis* fields (>0.5 km^2) and identifies perennial *aufeis* patches at the end of the ablation season and their occurrence over the last four decades using Landsat imagery.

2. Study Area

Covering an area of approximately 31,000 km^2, the endorheic PTB is located in the transition zone between the eastern Trans-Himalayan and Karakoram ranges of Ladakh and the western parts of the Tibetan Plateau (Figure 1). The study area is bounded by the Chang Chenmo mountain ranges in the north and the Pangong Range as well as the Kailash Range in the south, all with elevations up to 6600 m a.s.l. Between these mountain ranges, there is a plateau with wide valleys and tectonic basins [38] characterized by lakes of different sizes. The largest saline lake is Pangong Tso, which covers an area of approximately 680 km^2 at an elevation of 4225 m a.s.l. [39–42] (Figure 2). Pangong Tso and its tectonic continuation to the east divide the study area into a northern and a southern portion of almost equal sizes of 14,750 km^2 and 16,484 km^2, with mean elevations of 5083 m a.s.l. and 4912 m a.s.l., respectively.

The sparse vegetation is mainly confined to wetlands with moist alluvial and organic-rich soils around lakes, rivers, and streams. Hillslopes are sparsely vegetated, and desert steppe plant communities such as *Stipa*, *Oxytropis*, *Acantholimon lycopodioides*, *Thylacospermum caespitosum*, and *Kraschenninikovia ceratoides* are dominant [43,44]. Wetlands serve as seasonal grazing and resting areas for livestock [45] and as breeding habitat for birds [46]. Due to the harsh environmental conditions of the PTB, nomadic pastoralism has historically been the main source of livelihood [47–49]. Despite the disputed territoriality along the contested border region, which limits access for field surveys [50], the settlements along the southern and western shore of Pangong Tso have become tourism hotspots. Due to inadequate infrastructure, increased tourism has taken its toll on the fragile ecosystem [46,51,52].

Due to the cold-arid conditions, mean annual precipitation of about 100 mm, and annual temperatures ranging from −15 °C in January to 10 °C in July [53–57], the streams and rivers are mainly fed by meltwater from seasonal snow cover and high-altitude glaciers [58,59]. Due to massive morainic valley fills in these broad valleys resulting from the Pleistocene glaciation [42,60], water discharge varies between surface and subsurface runoff [61]. The resulting meltwater streams along the valleys create favorable conditions for *aufeis* formation. Especially in the northern portion of the PTB, large and wide valleys with low gradients and braided streams characterize the landscape. In contrast, the southern portion of the PTB is dominated by short and narrow valleys.

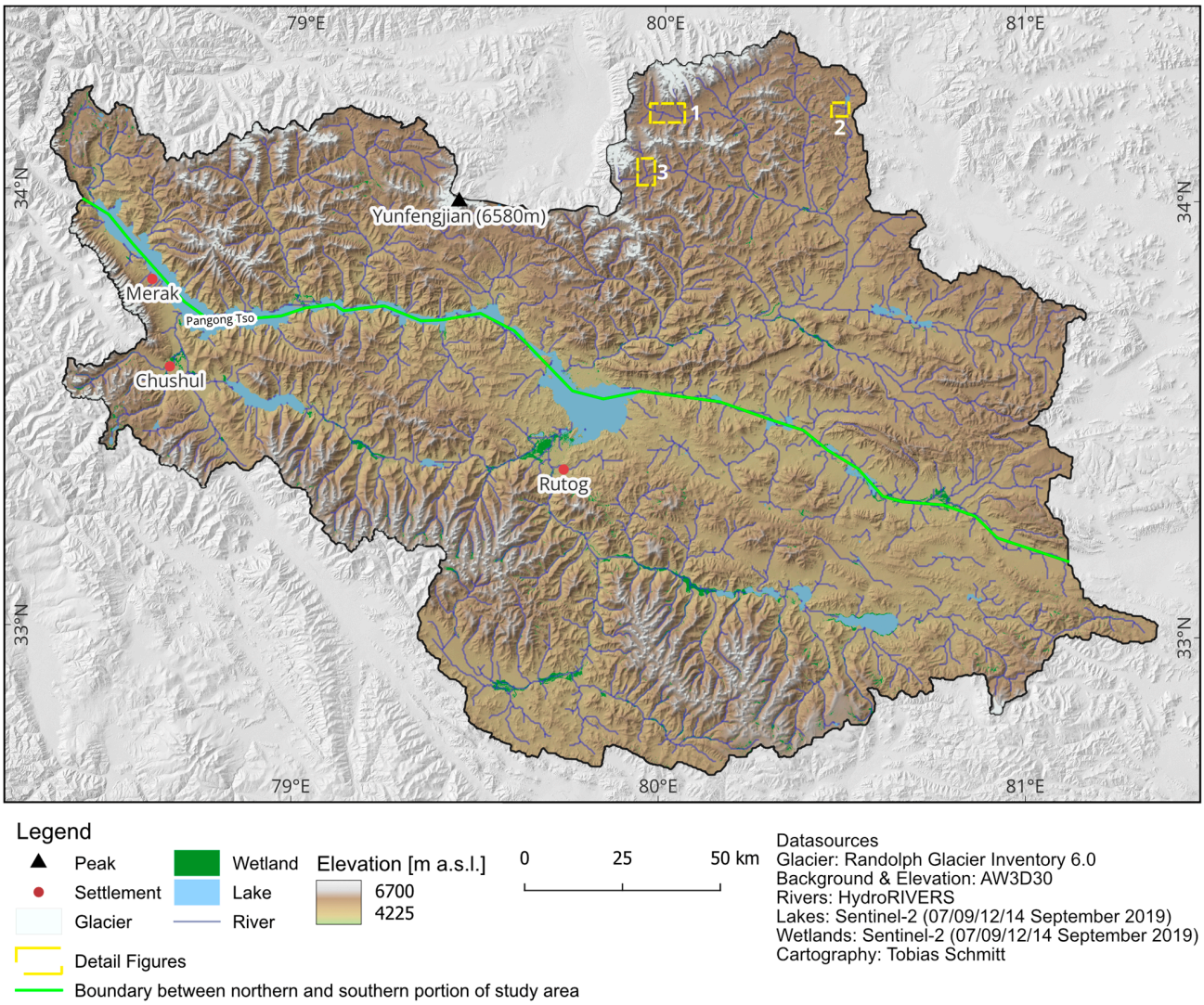


Figure 1. The Pangong Tso basin, Trans-Himalaya.



Figure 2. Broad valleys indicating thick sediment fills with dry surface channels on the northwestern shore of the Pangong Tso, eastern Ladakh (taken by Marcus Nüsser at 33°41′07″ N, 78°38′29″ E from 4375 m a.s.l. on 3 October 2022).

3. Materials and Methods

3.1. Materials

Cloud-free Sentinel-2 data from spring 2019 were applied for the *aufeis* inventory and from autumn 2019 for the identification of perennial *aufeis* fields in the study area. According to studies in the vicinity of the PTB [31,32], *aufeis* fields reach their maximum extent in May and can be easily separated from the surrounding snow- and ice-free land cover. The smallest ice-covered area occurs in early autumn. Due to frequent night-time temperatures below 0 °C, the accumulation process regularly starts in October. Level-1C products (top-of-atmosphere) of Sentinel-2 were used to avoid artefacts and oversaturation, which often occur in Level-2A (surface reflectance) products in arid mountainous areas. To reduce the number of misclassified pixels, only images with low snow cover were selected for further processing. Due to the size of the PTB, nine tiles from five different dates were used for each season (Table 1).

Table 1. Satellite imagery and digital elevation models and their derivates used for the detection and analysis of *aufeis* in the Pangong Tso Basin (PTB).

Dataset	Tiles	Acquisition Date (Spring)	Acquisition Date (Autumn)	Spatial Resolution	Spectral Resolution
Sentinel-2 [a]	T44SKC	10 May 2021	12 September 2019, 23 September 2023	10 m 20 m	VIS *, NIR * SWIR 1 *
	T44SLD	27 April 2019	14 September 2019, 23 September 2023		
	T44SLC	20 April 2019 7 May 2019	12/19 September 2019, 23 September 2023		
	T44SLB	5/7 May 2019	7/9 September 2019, 23 September 2023		
	T44SMD	5/7 May 2019	9 September 2019, 23 September 2023		
	T44SMC	5/7 May 2019	9 September 2019, 23 September 2023		
	T44SMB	5/7 May 2019	9 September 2019, 23 September 2023		
	T44SNC	20 April 2019	9 September 2019, 23 September 2023		
	T44SNB	7 May 2019	9 September 2019, 23 September 2023		
Landsat 5 [b]	145/037		24 September 1994	30 m	VIS *, NIR *
Landsat 7 [b]	145/037		29 September 1999		
Landsat 5 [b]	146/036		23 September 2023		
Landsat 8 [b]	146/036		8 September 2015		
ALOS World 3D/AW3D30 [c]	N033-34E078 N032-34E079 N032-34E080 N032-34E081			30 m	
Hydro SHEDS [d]	HydroBASINS HydroRIVERS				

* Abbreviation of satellite bands visible (VIS), near-infrared (NIR), and short-wave infrared 1 (SWIR1). [a] https://dataspace.copernicus.eu/browser/ (accessed on 19 October 2023); [b] https://earthexplorer.usgs.gov/ (accessed on 19 October 2023); [c] https://www.eorc.jaxa.jp/ALOS/en/dataset/aw3d30/aw3d30_e.htm (accessed on 19 October 2023); [d] https://www.hydrosheds.org/ (accessed on 20 October 2023).

To further analyze the potential persistence of individual *aufeis* fields over the recent decades, Landsat imagery was integrated as an additional data source, as it is the only available satellite data that can be used for comparison with high spatial resolution over decadal observations. However, cloud cover and partial data gaps due to ground station malfunction over the HMA limited the suitable time intervals [32]. Therefore, four Landsat

datasets from September 1994, 1999, 2009, and 2015 and Sentinel-2 images from 2023 were selected.

The ALOS Global Digital Surface Model (AW3D30) with a spatial resolution of 30 m was used as an additional input for the classification and for the estimation of topographic parameters such as elevation, slope, and aspect of *aufeis*. The endorheic PTB was delineated from the HydroBASINS datasets of the HydroSHEDS project. Streams and rivers were extracted from the HydroRIVERS dataset [62].

3.2. Methods

The Sentinel-2 tiles were mosaicked and resampled to a spatial resolution of 10 m for visual interpretation and to a spatial resolution of 30 m for comparative mapping purposes with other *aufeis* inventories using Landsat imagery [24,29–33,63] and to match the spatial resolution of the AW3D30. The mosaicked satellite images were classified using a decision tree approach, which is based on a series of binary decisions with predefined thresholds that assign each pixel to a distinct class (Figure 3). The advantage of this approach lies in the individual setting of thresholds and in its easy reproducibility. It is commonly used in *aufeis* detection [24,29,31,33] and glacier mapping [64–67].

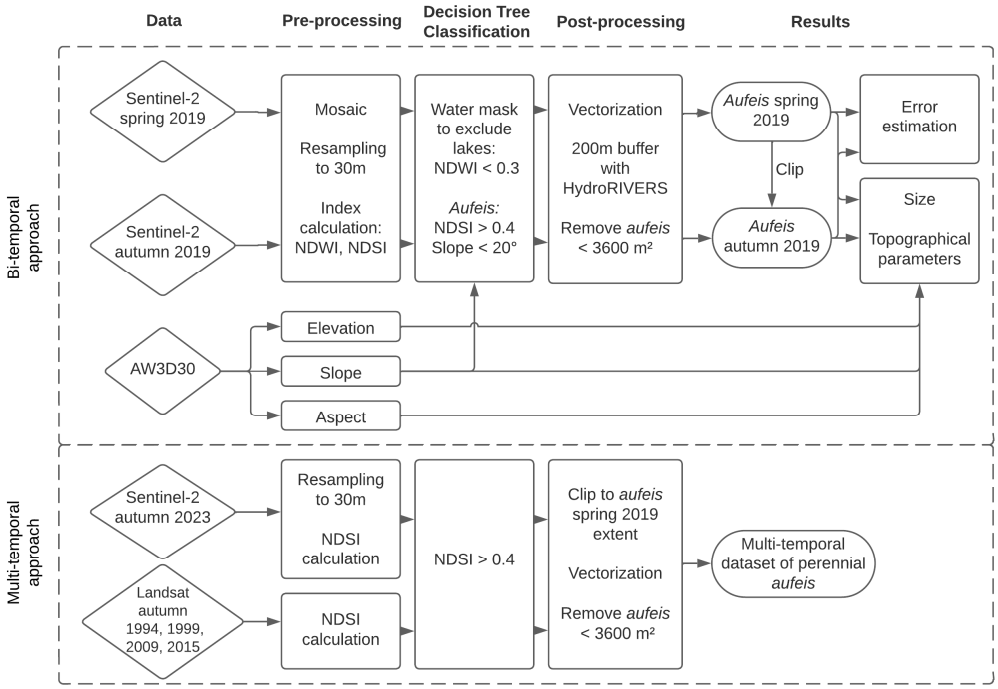


Figure 3. Flowchart showing the data and methodology used to map and inventory seasonal *aufeis* fields in the Pangong Tso Basin (PTB) in 2019 and to investigate the occurrence of perennial *aufeis* fields since 1994.

For the first node of the decision tree, the Normalized Difference Water Index (NDWI) [68] was utilized:

$$NDWI = \frac{Green - NIR}{Green + NIR} \quad (1)$$

A threshold of <0.3 was set to mask the lakes in the PTB. In the second and third decisions, the Normalized Difference Snow Index (NDSI) [69] was utilized:

$$NDSI = \frac{Green - SWIR1}{Green + SWIR1} \quad (2)$$

A threshold of >0.4 and a slope angle of < 20° derived from the AW3D30were used to separate pixels covered by *aufeis* from snow. Inventories of the neighboring regions indicate that the majority of *aufeis* fields are located on slopes of less than 10° [31–33]. As most of

the *aufeis* fields occur in the vicinity of rivers and streams, the HydroRIVERS dataset was used with a buffer of 200 m to further eliminate misclassifications, for example, caused by seasonal snow cover, especially in the upper catchments.

The classified *aufeis* pixels were converted into vector features. Remaining misclassifications in the transition zone between the valley floor and adjacent slopes were manually removed. *Aufeis* located outside the buffer were manually added. *Aufeis* fields with an area of less than four Landsat pixels (3600 m^2) were removed to ensure comparability with other datasets [28,32]. The mapped *aufeis* fields were divided into two distinct areas: the northern and the southern portion of the PTB. The topographic parameters of all *aufeis* fields, such as elevation, slope, and aspect, were derived from AW3D30 on a pixel-by-pixel basis.

The Sentinel-2 imagery of autumn 2019 were classified in order to map the occurrence of perennial *aufeis* fields. For this purpose, the spring 2019 *aufeis* extent was used as a clipping mask. In order to investigate their persistence over several time periods, the five Landsat images from September 1994, 1999, 2009, and 2015 as well as the Sentinel-2 image from 2023 were classified using the NDSI threshold and clipped to the spring 2019 *aufeis* extent. Subsequently, *aufeis* fields smaller than 3600 m^2 were removed.

In the final step, the uncertainty was estimated with a half-pixel buffer for each *aufeis* field (±15 m). The error estimation was calculated by the standard deviation of the sum of the error for each *aufeis* field [31]. Further field-based accuracy assessments using in situ observations and measurements were not possible due to restricted access along the disputed border. However, field surveys and measurements were conducted in the Upper Indus Basin (UIB) and the Tso Moriri Basin in the immediate vicinity of the PTB in the winters of 2014, 2016, 2023, and 2024.

4. Results

The *aufeis* distribution shows a distinct concentration along the rivers and streams that drain the glacierized mountain ranges in the southern and northern portions of the PTB. The characteristic locations of *aufeis* fields in the northern portion of the study area are illustrated in Figure 4.

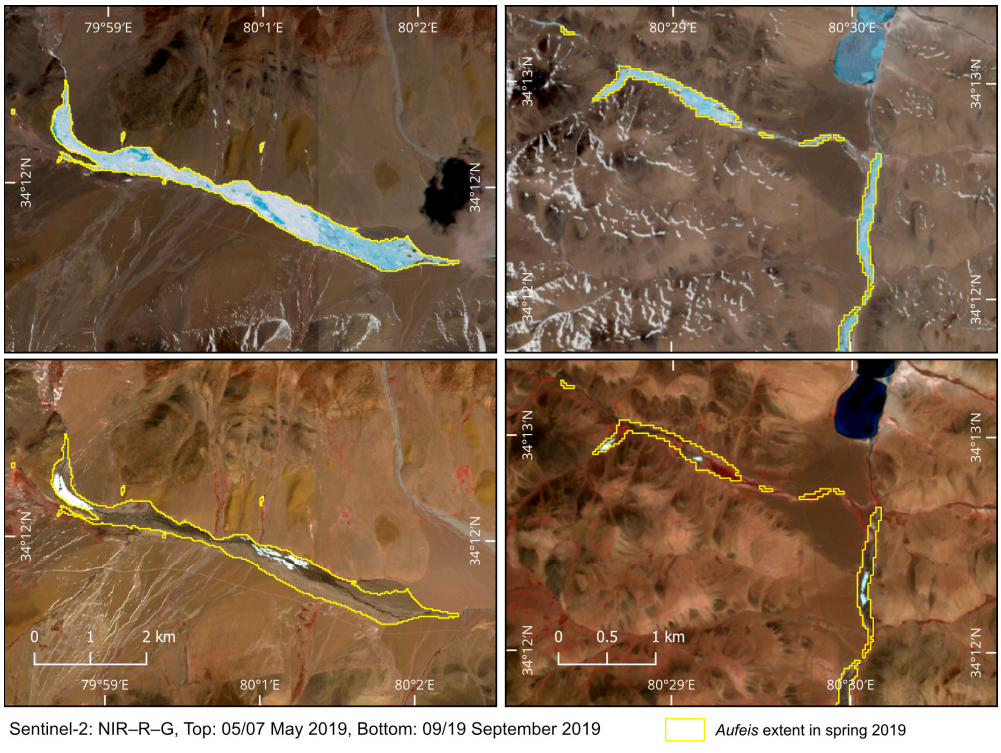


Figure 4. *Aufeis* fields in spring 2019 (**top**), which partly exist as fragmented patches until the end of the ablation period in September 2019 (**bottom**). Left: An *aufeis* field (2.88 km^2) (yellow rectangle no. 1

in Figure 1) at an elevation of 5050–5070 m a.s.l. divided into three patches of 0.14 km^2, 0.08 km^2, and 0.04 km^2, respectively. Right: The example (yellow rectangle no. 2 in Figure 1) shows that the northern *aufeis* field (0.21 km^2) at an elevation of 5100–5200 m a.s.l. divided into two patches, while the smaller southern field of 0.15 km^2 shrunk to 0.02 km^2.

In the northeastern part of PTB, an area of about 41 km^2 was covered by *aufeis*, where a braided river system was established, forming a cascading sequence of *aufeis* fields. In this area, the largest *aufeis* field with an area of 14.8 ± 0.01 km^2 was detected along a broad valley in the northern portion. It is striking that almost no *aufeis* fields were detected in the eastern part of PTB (Figure 5).

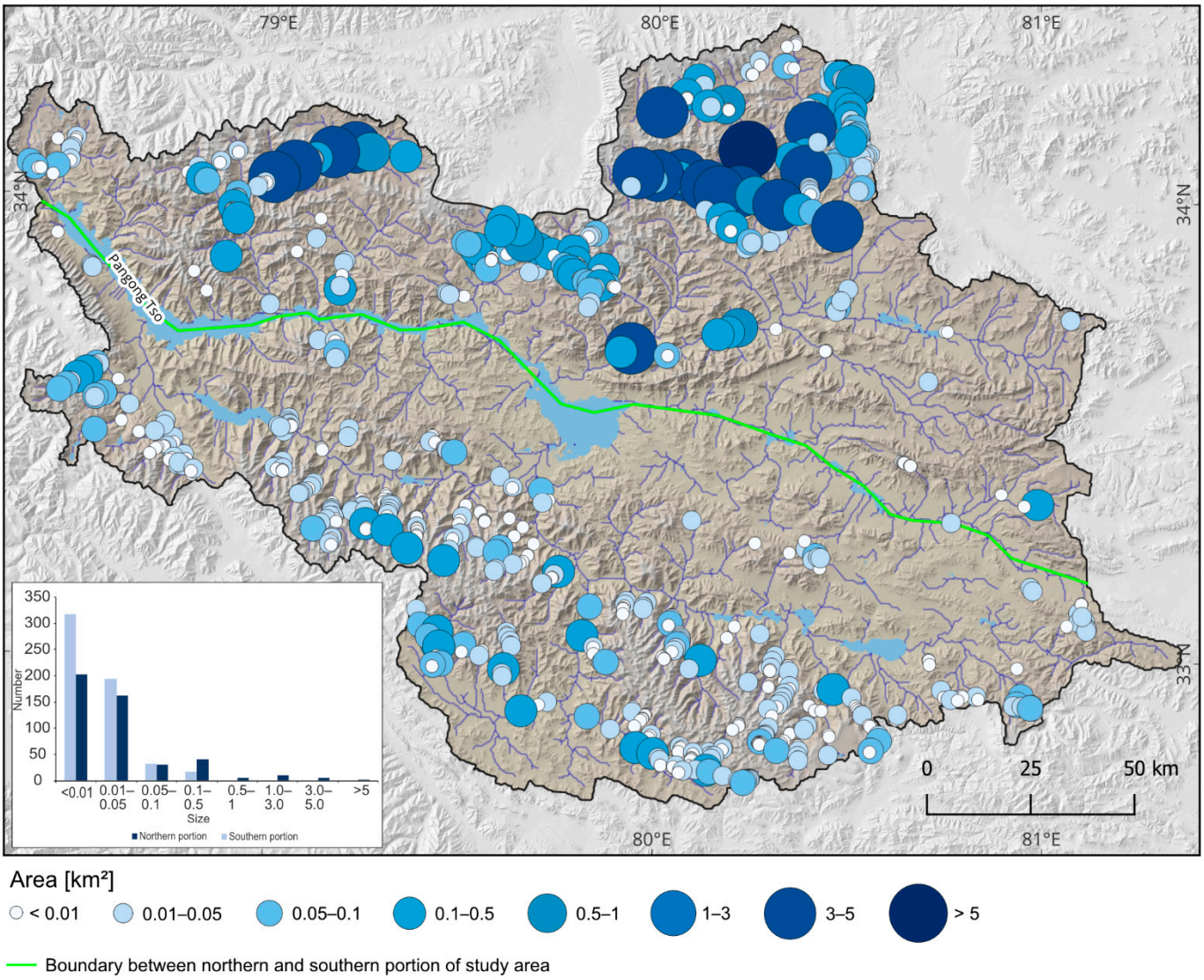


Figure 5. Spatial distribution and size of *aufeis* fields in the study area of Pangong Tso Basin (PTB) in spring 2019.

In total, 1022 *aufeis* fields were detected in spring 2019, covering an area of 85.6 ± 0.07 km^2 with an average size of 0.08 km^2. Overall, 86% of them were smaller than 0.05 km^2 and covered an area of only 10.5 ± 0.01 km^2, while 82 were larger than 0.1 km^2, accounting for 82% (70.8 ± 0.19 km^2) of the total area. Twenty-three individual *aufeis* fields were even larger than 0.5 km^2; these are considered giant *aufeis* according to the threshold used by Ensom et al. [28]. Their spatial distribution was strictly limited to the northern portion of

the PTB. This results in a striking contrast between the northern and southern portions, as 74.2 ± 0.09 km^2 or 87% of the total *aufeis*-covered area was located in the northern portion, although only less than half of all individual *aufeis* fields were located there. This difference is also apparent in their average size: 0.02 km^2 and 0.16 km^2 in the southern and northern portions, respectively.

The elevation distribution of all *aufeis*-covered areas ranged from 4250–5600 m a.s.l. (Figure 6). In total, 53% of these areas were located between 4800 m a.s.l. and 5100 m a.s.l., with a slight increase in elevation towards the north. Thus, in the northern portion, 34 km^2 of the area covered by *aufeis* was located in the elevation range 4900–5100 m a.s.l., while in the southern portion, most of the *aufeis* was located between 4700 m a.s.l. and 4900 m a.s.l. Accordingly, the average elevation in the northern portion is almost 100 m higher than in the southern portion, where the average elevation is 4860 m a.s.l. Giant *aufeis* fields are restricted to the elevation range 4800–5100 m a.s.l.

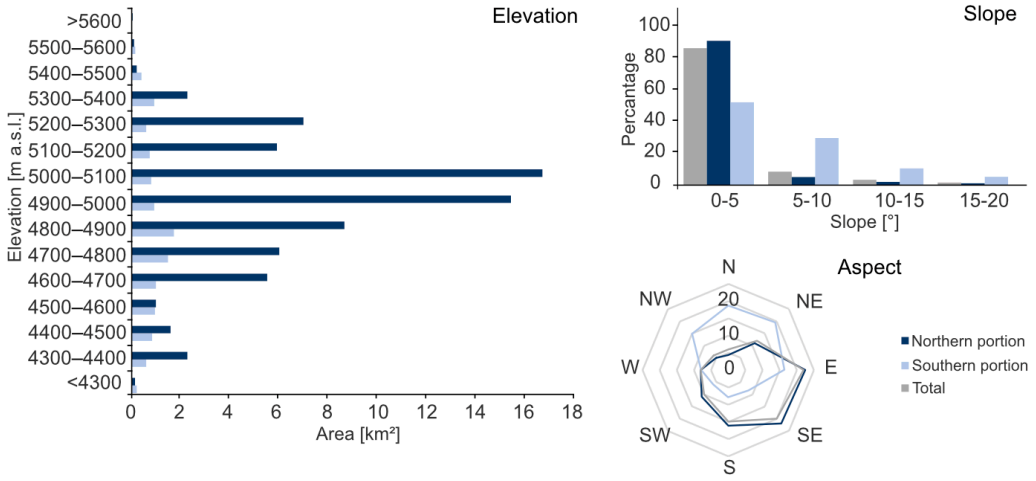


Figure 6. Elevation, slope, and aspect of *aufeis*-covered area in the Pangong Tso Basin (PTB) in spring 2019.

We found that 87% of the *aufeis*-covered area in the PTB was located on gentle slopes of less than 5° (Figure 6). In the northern portion of PTB, 90% of the ice-covered area belonged to this slope class, whereas in the southern portion, only 50% belonged to this class. However, the percentage of *aufeis* (10%) on slopes steeper than 10° was higher in the southern than in the northern portion (2%).

Approximately 60% of the total *aufeis* area was located on east-, southeast-, and south-facing slopes (Figure 6). While the distribution in the northern portion was predominantly southeast- and east-facing, only 5 to 10% of ice-covered areas in the southern portion belonged to this class. Instead, almost 20% of the ice-covered area faced north and northeast.

In total, 14 *aufeis* fields had not completely melted and had fragmented into 29 smaller patches by autumn 2019 (Figure 7). The remaining patches covered an area of 1.2 ± 0.02 km^2, with an average size of 0.04 km^2. Almost half of these patches belonged to the size class 0.01–0.05 km^2, while four of them were larger than 0.1 km^2 and covered a total area of 0.75 ± 0.01 km^2. All of these perennial *aufeis* patches were located in the northern portion above 5000 m a.s.l., while 74% of the area was between 5200 and 5400 m a.s.l. Overall, the mean elevation was almost 300 m higher in autumn than in spring, amounting to 5272 m a.s.l. compared to 4935 m a.s.l., respectively. Furthermore, the perennial *aufeis* patches were predominantly located on east-, southeast-, and south-facing slopes with a gradient of less than 5° (Figure S1).

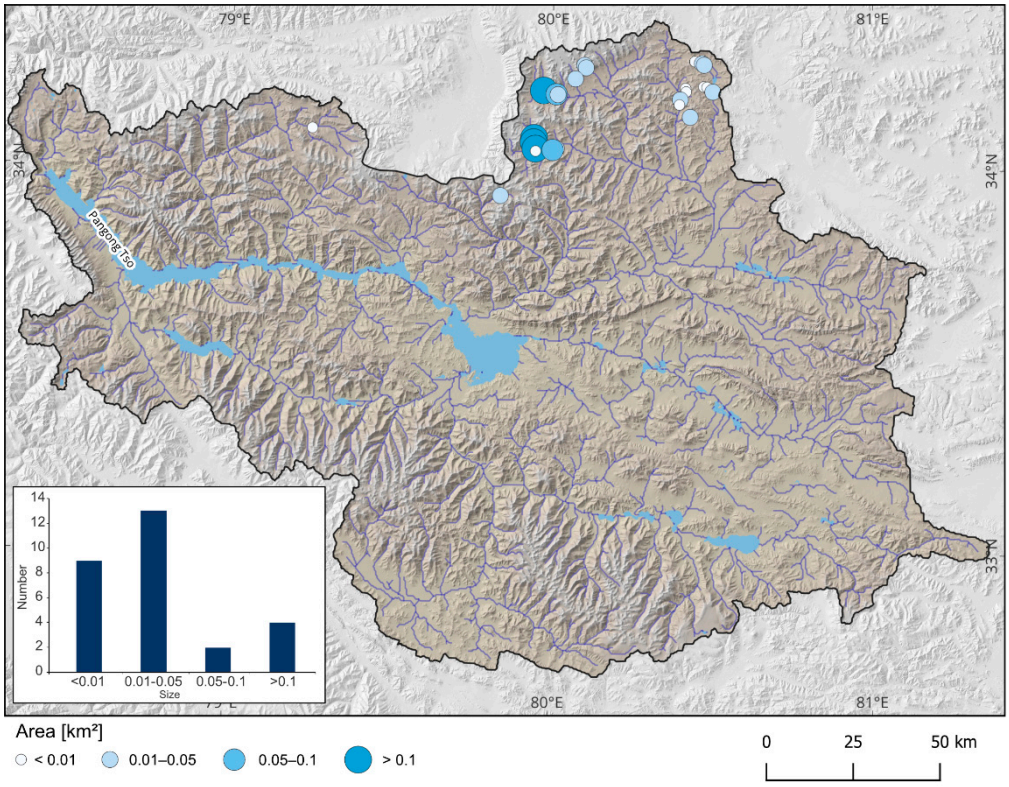


Figure 7. Spatial distribution and size of *aufeis* in autumn 2019.

The multi-temporal comparison between 1994 and 2023 (Figure 8 and Figure S2) shows that the number of remaining *aufeis* fields varied between 8 and 29, with the largest number in 2019. The total area ranged from around 0.3 km^2 in 1994 and 2023 to around 1.2 km^2 in 2015 and 2019. There is, therefore, no clear decreasing or increasing trend. The size of the largest remaining individual *aufeis* patches varied between 0.09 km^2 in 2023 and 0.22 km^2 in 2015. However, the remaining patches were almost always located in the same places, indicating similar melting patterns from year to year.

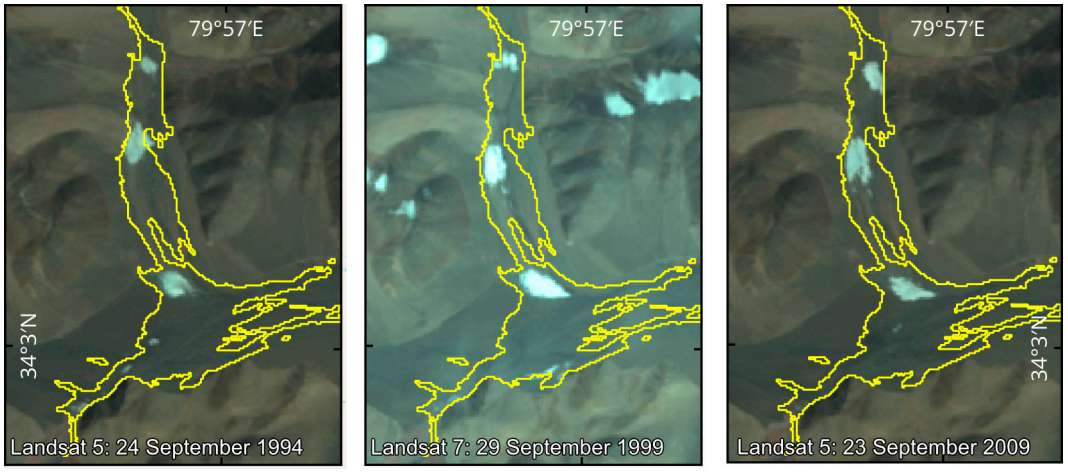


Figure 8. *Cont.*

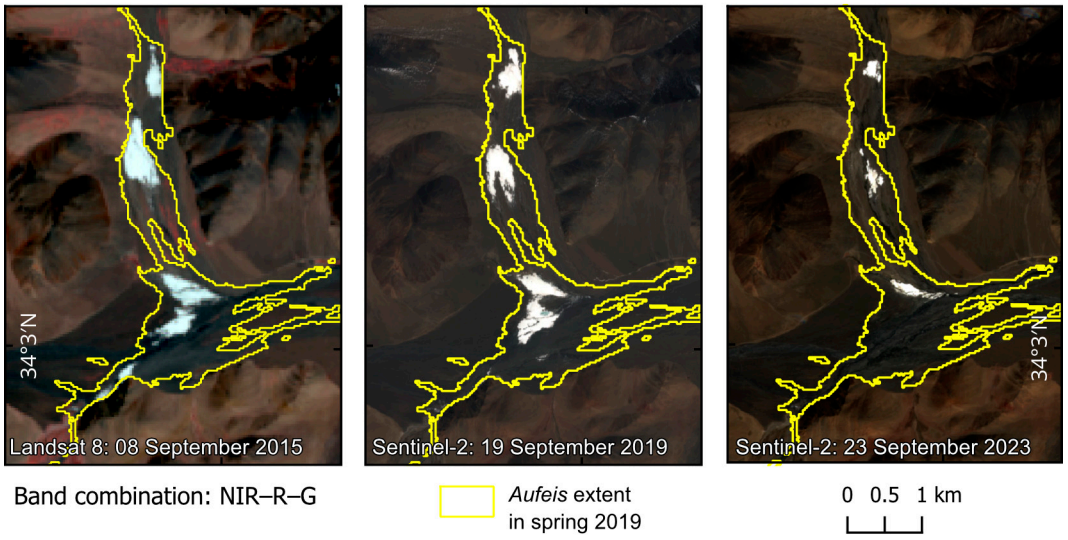


Figure 8. Patterns of remaining *aufeis* fields, which follow almost the same spatial structures each year.

5. Discussion

The semi-automatic remote sensing approach enables the detection of *aufeis* in cold-arid environments, as the generally low amount of snow cover reduces the risk of misclassification, which is further minimized by the use of a buffer mask along the rivers and a maximum slope gradient of 20°. Thus, manual corrections are required to detect groundwater-fed *aufeis* on slopes > 20°. The selected observation period controls the detected amount and size of *aufeis*. In contrast to glacier inventories, where the end of the ablation season in a given year is chosen to determine the extent of the glacier, the time used to map the maximum extent of *aufeis* varies and ranges from early spring (March) to early summer (June) [24,29,32,33,70], which may be further influenced by the availability of suitable optical satellite imagery. The increasing availability of (free) optical remote sensing imagery has the potential to contribute to efforts to produce spatially consistent maps of *aufeis*, to quantify *aufeis* distribution on regional and global scales, and to better understand its environmental [71] and socio-hydrological [18,72] importance, both of which have been largely overlooked in research.

In the cold-arid PTB, more than 1000 *aufeis* fields were mapped, covering an area of 86 km^2. As in the UIB, where an increasing number of *aufeis* fields towards the east were detected, these observations underline the fact that cold-arid conditions without thick seasonal snow cover provide the most favorable conditions for *aufeis* formation [26,73].

The elevation distribution of *aufeis* fields in the endorheic PTB is similar to the adjacent larger UIB, where most *aufeis* fields are located between 4900–5000 m a.s.l. [31]. However, in the neighboring Kunlun Mountains, the maximum of *aufeis* area is located at lower elevations between 4000 m a.s.l. and 4400 m a.s.l. [33]. In this elevation range, almost no *aufeis* has been identified in the PTB, although it represents the third-largest elevation range in the basin. These relatively low-lying areas are mainly located in the eastern part and in close proximity to Pangong Tso. In this area, ice formation is mostly confined to isolated, sporadic patches adjacent to the saline lakes, probably also caused by the lack of perennial streams. Similar patterns have already been described in early exploration reports [51], where the absence of streams in the vicinity of the lakes were mentioned. In the same text, Godwin-Austen assumed that water flows over the surface of ice-covered lakes in winter, when the pressure becomes too high, resulting in an overflow and the formation of thick layers of ice along the shores.

A significant difference in the size of *aufeis* fields between the northern and southern portions of the PTB is a characteristic feature of the regional cryosphere (Figure 5). Following the approach of Ensom et al. [28], 23 *aufeis* fields in spring could be considered as giant

aufeis (>0.5 km^2); all of them were located in the northern portion of the PTB, whereas none of the remaining *aufeis* patches exceeded this threshold. A major reason for this striking contrast can be attributed to topographic factors. Broad valleys and braided river systems are mostly located in the northern portion of the PTB. Such geomorphological settings are considered favorable for the development of large *aufeis* fields [74,75]. The wide and shallow valley bottoms, where discharge can fluctuate between surface and subsurface flow, favor freezing to the bottom of the stream, leading to a blockage of the streamflow, which results in an increase in hydrostatic pressure and overflow of water to the surface. Visual verification using high-resolution Google Earth imagery as well as Sentinel-2 imagery revealed clearly identifiable water sources percolating through the riverbed sediments. Similar patterns have already been observed in the endorheic Tso Moriri Basin, located to the south of the PTB, where the size of the *aufeis* fields ranges from 0.007–1.7 km^2 [32]. In contrast, the rugged topography and narrow valleys in the southern portion of the PTB result in smaller *aufeis* fields, which can also be detected in the UIB [31]. In addition to the river morphology, the glacierized area is substantially larger in the northern than in the southern portion of the PTB. This leads to an increased meltwater runoff, which may contribute to groundwater recharge in spring and summer. The *aufeis* can therefore be seen as an indicator of complex surface–groundwater interactions in this permafrost environment [76].

Although giant *aufeis* are usually associated with sub-permafrost water sources, supra-permafrost perennial groundwater systems in a talik may also contribute to large *aufeis* formation [77,78]. The presence of taliks along the streams in the PTB cannot be verified due to the lack of field-based in situ data; their occurrence remains an open question. Research on the interactions between the thickness of *aufeis* and the associated talik would contribute to an improved understanding of cryo-hydrological processes in the permafrost zone in order to predict changes in *aufeis* dynamics in HMA. Changes have already been observed in other *aufeis*-affected regions, where the number and size of large *aufeis* fields are decreasing [24,27,29,79].

Persisting *aufeis* in autumn can already be observed on historical photographs from the 19th and first half of the 20th century [35–37] in and around the PTB, but they have not been detected in remote sensing data. In the present study, several enduring *aufeis* patches were identified in the northern portion of the PTB in autumn 2019. All of them were remnant patches of spring 2019 *aufeis* fields larger than 0.5 km^2, while the largest *aufeis* field from the same observation had completely disappeared. A first visual assessment of remnant *aufeis* fields in the PTB over the observation period 1994–2023 provides evidence that these remaining patches were almost always located at the same topographic locations. It also demonstrates that site-specific characteristics facilitate the development of ice bodies that are thick enough to withstand the ice loss through melting and sublimation. While remote sensing data provide valuable insights into the *aufeis* conditions in the region, it remains difficult to explain the exact factors contributing to the persistence of the ice patches at the specific locations solely based on satellite imagery. Therefore, in situ investigations are essential to further elucidate the complex mechanisms for *aufeis* formation [28].

6. Conclusions

In this study, *aufeis* occurrence in the PTB was mapped using Sentinel-2 imagery from 2019 in spring and autumn based on a semi-automatic decision tree approach. In total, the *aufeis* covered an area of 86 km^2 in spring, with elevations ranging from 4200–5700 m a.s.l. A striking contrast in *aufeis* formation was detected between the northern and the southern portions of the PTB and was caused by differences in geomorphological settings, mainly the presence of broad valley floors north of Pangong Tso. In the northern portion, 23 individual *aufeis* fields were larger than 0.5 km^2 in spring and were considered as giant *aufeis*. By the end of the ablation period in 2019, 14 *aufeis* fields had not completely melted and were fragmented into 29 smaller *aufeis* patches, some of which had been detected in the same locations in different years since 1994. This study is a further contribution to ongoing efforts

to map *aufeis* in the cold-arid regions of HMA. It complements existing inventories and closes the gap towards the Tibetan Plateau, where extensive *aufeis* formation is expected.

Supplementary Materials: The following supporting information can be downloaded at: https://www.mdpi.com/article/10.3390/atmos15030263/s1, Figure S1: Elevation, slope, and aspect of *aufeis* in Pangong Tso Basin (PTB) in autumn 2019; Figure S2: Reoccurring spatial pattern of remaining *aufeis* fields in the northern portion of the Pangong Tso Basin (PTB) between 1994 and 2023.

Author Contributions: Conceptualization, T.S., D.B., S.S. and M.N.; methodology, T.S. and D.B.; software, D.B. and T.S.; validation, T.S.; formal analysis, T.S. and D.B.; investigation, T.S., D.B. and S.S.; resources, M.N.; data curation, S.S., M.N. and D.B.; writing—original draft preparation, T.S., D.B. and S.S.; writing—review and editing, M.N.; visualization, T.S., D.B. and S.S.; supervision, S.S. and M.N.; project administration, M.N.; funding acquisition, M.N. All authors have read and agreed to the published version of the manuscript.

Funding: This research was funded by the German Research Foundation (DFG) in the context of the project NU102/15-1.

Institutional Review Board Statement: Not applicable.

Informed Consent Statement: Not applicable.

Data Availability Statement: The data that support the findings of this study are available from the corresponding author upon reasonable request. The entire inventory of the Upper Indus Basin (UIB), Tso Moriri Basin (TMB), and Pangong Tso Basin (PTB) will be published in a data journal.

Acknowledgments: The authors are thankful to the German Research Foundation (DFG) for their financial support and to USGS and ESA for making satellite data freely available to users. The authors acknowledge support by the state of Baden-Württemberg through SDS for data storage. An earlier version of this study was presented at the General Assembly of the European Geoscience Union (EGU) in April 2023 (CR5.2). The authors are grateful to the four anonymous reviewers for their constructive comments that helped to improve the article.

Conflicts of Interest: The authors declare no conflict of interest.

References

1. Hock, R.; Rasul, G.; Adler, C.; Cáceres, B.; Gruber, S.; Hirabayashi, Y.; Jackson, M.; Kääb, A.; Kang, S.; Kutuzov, S.; et al. High Mountain Areas. In *IPCC Special Report on the Ocean and Cryosphere in a Changing Climate*; Pörtner, H.-O., Roberts, D.C., Masson-Delmotte, V., Zhai, P., Tignor, M., Poloczanska, E., Mintenbeck, K., Alegría, A., Nicolai, M., Okem, A., et al., Eds.; Cambridge University Press: Cambridge, UK; New York, NY, USA, 2019; pp. 131–202. [CrossRef]
2. Barnett, T.P.; Adam, J.C.; Lettenmaier, D.P. Potential Impacts of a Warming Climate on Water Availability in Snow-Dominated Regions. *Nature* **2005**, *438*, 303–309. [CrossRef]
3. Immerzeel, W.W.; Lutz, A.F.; Andrade, M.; Bahl, A.; Biemans, H.; Bolch, T.; Hyde, S.; Brumby, S.; Davies, B.J.; Elmore, A.C.; et al. Importance and Vulnerability of the World's Water Towers. *Nature* **2020**, *577*, 364–369. [CrossRef]
4. Viviroli, D.; Kummu, M.; Meybeck, M.; Kallio, M.; Wada, Y. Increasing Dependence of Lowland Populations on Mountain Water Resources. *Nat. Sustain.* **2020**, *3*, 917–928. [CrossRef]
5. Kaser, G.; Großhauser, M.; Marzeion, B. Contribution Potential of Glaciers to Water Availability in Different Climate Regimes. *Proc. Natl. Acad. Sci. USA* **2010**, *107*, 20223–20227. [CrossRef]
6. Carey, M.; Molden, O.C.; Rasmussen, M.B.; Jackson, M.; Nolin, A.W.; Mark, B.G. Impacts of Glacier Recession and Declining Meltwater on Mountain Societies. *Ann. Am. Assoc. Geogr.* **2017**, *107*, 350–359. [CrossRef]
7. Mukherji, A.; Sinisalo, A.; Nüsser, M.; Garrard, R.; Eriksson, M. Contributions of the Cryosphere to Mountain Communities in the Hindu Kush Himalaya: A Review. *Reg. Environ. Chang.* **2019**, *19*, 1311–1326. [CrossRef]
8. Parveen, S.; Winiger, M.; Schmidt, S.; Nüsser, M. Irrigation in Upper Hunza: Evolution of Socio-Hydrological Interactions in the Karakoram, Northern Pakistan. *Erdkunde* **2015**, *69*, 69–85. [CrossRef]
9. Nüsser, M.; Schmidt, S. Nanga Parbat Revisited: Evolution and Dynamics of Socio-Hydrological Interactions in the Northwestern Himalaya. *Ann. Am. Assoc. Geogr.* **2017**, *107*, 403–415. [CrossRef]
10. Armstrong, R.L.; Rittger, K.; Brodzik, M.J.; Racoviteanu, A.; Barrett, A.P.; Khalsa, S.-J.S.; Raup, B.; Hill, A.F.; Khan, A.L.; Wilson, A.M.; et al. Runoff from Glacier Ice and Seasonal Snow in High Asia: Separating Melt Water Sources in River Flow. *Reg. Environ. Chang.* **2019**, *19*, 1249–1261. [CrossRef]
11. Hugonnet, R.; McNabb, R.; Berthier, E.; Menounos, B.; Nuth, C.; Girod, L.; Farinotti, D.; Huss, M.; Dussaillant, I.; Brun, F.; et al. Accelerated Global Glacier Mass Loss in the Early Twenty-First Century. *Nature* **2021**, *592*, 726–731. [CrossRef] [PubMed]

12. Rounce, D.R.; Hock, R.; Maussion, F.; Hugonnet, R.; Kochtitzky, W.; Huss, M.; Berthier, E.; Brinkerhoff, D.; Compagno, L.; Copland, L.; et al. Global Glacier Change in the 21st Century: Every Increase in Temperature Matters. *Science* **2023**, *379*, 78–83. [CrossRef]
13. Dharpure, J.K.; Goswami, A.; Patel, A.; Kulkarni, A.V. Snehmani Assessment of Snow Cover Variability and Its Sensitivity to Hydrometeorological Factors in the Karakoram and Himalayan Region. *Hydrol. Sci. J.* **2021**, *66*, 2198–2215. [CrossRef]
14. Notarnicola, C. Hotspots of Snow Cover Changes in Global Mountain Regions over 2000–2018. *Remote Sens. Environ.* **2020**, *243*, 111781. [CrossRef]
15. Biskaborn, B.K.; Smith, S.L.; Noetzli, J.; Matthes, H.; Vieira, G.; Streletskiy, D.A.; Schoeneich, P.; Romanovsky, V.E.; Lewkowicz, A.G.; Abramov, A.; et al. Permafrost Is Warming at a Global Scale. *Nat. Commun.* **2019**, *10*, 264. [CrossRef] [PubMed]
16. Gruber, S.; Fleiner, R.; Guegan, E.; Panday, P.; Schmid, M.-O.; Stumm, D.; Wester, P.; Zhang, Y.; Zhao, L. Review Article: Inferring Permafrost and Permafrost Thaw in the Mountains of the Hindu Kush Himalaya Region. *Cryosphere* **2017**, *11*, 81–99. [CrossRef]
17. Nüsser, M.; Baghel, R. Local Knowledge and Global Concerns: Artificial Glaciers as a Focus of Environmental Knowledge and Development Interventions. In *Ethnic and Cultural Dimensions of Knowledge*; Meusburger, P., Freytag, T., Suarsana, L., Eds.; Knowledge and Space; Springer: Cham, Switzerland, 2016; pp. 191–209. ISBN 978-3-319-21900-4. [CrossRef]
18. Nüsser, M.; Dame, J.; Kraus, B.; Baghel, R.; Schmidt, S. Socio-Hydrology of "Artificial Glaciers" in Ladakh, India: Assessing Adaptive Strategies in a Changing Cryosphere. *Reg. Environ. Chang.* **2019**, *19*, 1327–1337. [CrossRef]
19. Nüsser, M.; Dame, J.; Parveen, S.; Kraus, B.; Baghel, R.; Schmidt, S. Cryosphere-Fed Irrigation Networks in the Northwestern Himalaya: Precarious Livelihoods and Adaptation Strategies Under the Impact of Climate Change. *Mt. Res. Dev.* **2019**, *39*, R1–R11. [CrossRef]
20. Clouse, C. Frozen Landscapes: Climate-Adaptive Design Interventions in Ladakh and Zanskar. *Landsc. Res.* **2016**, *41*, 821–837. [CrossRef]
21. Carey, K.L. *Icings Developed from Surface Water and Ground Water*; Cold Reg. Res. Eng. Monogr. III-D3; US Army Cold Regions Research and Engineering Laboratory: Hanover, NH, USA, 1973.
22. Barry, R.G.; Gan, T.Y. *The Global Cryosphere: Past, Present, and Future*, 2nd ed.; Cambridge University Press: Cambridge, UK, 2022; ISBN 978-1-108-48755-9.
23. Harris, S.; French, H.; Heginbottom, J.; Johnston, G.; Ladanyi, B.; Sego, D.; Everdingen, R. *Glossary of Permafrost and Related Ground-Ice Terms*; National Research Council of Canada, Associate Committee on Geotechnical Research, Permafrost Subcommittee: Ottawa, ON, Canada, 1988; p. 159. [CrossRef]
24. Morse, P.D.; Wolfe, S.A. Geological and Meteorological Controls on Icing (Aufeis) Dynamics (1985 to 2014) in Subarctic Canada. *J. Geophys. Res. Earth Surf.* **2015**, *120*, 1670–1686. [CrossRef]
25. Woo, M.-K. *Permafrost Hydrology*; Springer: Berlin/Heidelberg, Germany, 2012; ISBN 978-3-642-23461-3. [CrossRef]
26. Alekseev, V.R. Long-term variability of the spring taryn-aufeises. *Ice Snow* **2016**, *56*, 73–92. [CrossRef]
27. Zemlianskova, A.; Makarieva, O.; Shikhov, A.; Alekseev, V.; Nesterova, N.; Ostashov, A. The Impact of Climate Change on Seasonal Glaciation in the Mountainous Permafrost of North-Eastern Eurasia by the Example of the Giant Anmangynda Aufeis. *Catena* **2023**, *233*, 107530. [CrossRef]
28. Ensom, T.; Makarieva, O.; Morse, P.; Kane, D.; Alekseev, V.; Marsh, P. The Distribution and Dynamics of Aufeis in Permafrost Regions. *Permafr. Periglac. Process.* **2020**, *31*, 383–395. [CrossRef]
29. Makarieva, O.; Shikhov, A.; Nesterova, N.; Ostashov, A. Historical and Recent Aufeis in the Indigirka River Basin (Russia). *Earth Syst. Sci. Data* **2019**, *11*, 409–420. [CrossRef]
30. Makarieva, O.; Nesterova, N.; Shikhov, A.; Zemlianskova, A.; Luo, D.; Ostashov, A.; Alexeev, V. Giant Aufeis—Unknown Glaciation in North-Eastern Eurasia According to Landsat Images 2013–2019. *Remote Sens.* **2022**, *14*, 4248. [CrossRef]
31. Brombierstäudl, D.; Schmidt, S.; Nüsser, M. Distribution and Relevance of Aufeis (Icing) in the Upper Indus Basin. *Sci. Total Environ.* **2021**, *780*, 146604. [CrossRef] [PubMed]
32. Brombierstäudl, D.; Schmidt, S.; Nüsser, M. Spatial and Temporal Dynamics of *Aufeis* in the Tso Moriri Basin, Eastern Ladakh, India. *Permafr. Periglac. Process.* **2023**, *34*, 81–93. [CrossRef]
33. Gagarin, L.; Wu, Q.; Cao, W.; Jiang, G. Icings of the Kunlun Mountains on the Northern Margin of the Qinghai-Tibet Plateau, Western China: Origins, Hydrology and Distribution. *Water* **2022**, *14*, 2396. [CrossRef]
34. Kamp, U.; Walther, M.; Dashtseren, A. Mongolia's Cryosphere. *Geomorphology* **2022**, *410*, 108202. [CrossRef]
35. Strachey, H. Physical Geography of Western Tibet. *J. R. Geogr. Soc. Lond.* **1853**, *23*, 1–69. [CrossRef]
36. De Terra, H. Physiographic Results of a Recent Survey in Little Tibet. *Geogr. Rev.* **1934**, *24*, 12–41. [CrossRef]
37. Hedin, S.A. *Im Herzen von Asien*; Brockhaus: Leipzig, Germany, 1903; Volume 2.
38. Srikantiai, S.V.; Ganesan, T.M.; Wangdus, C. A Note on the Tectonic Framework and Geologic Set-up of the Pangong-Chushul Sector, Ladakh Himalaya. *J. Geol. Soc. India* **1982**, *2*, 354–357.
39. Bhat, H.; Mahapatra, D.M.; Rao, S.; Ramachandra, T.V. *Avian Diversity of Ladakh Wetlands*; ENERGY and Wetlands Research Group, Centre for Ecological Sciences, Indian Institute of Science: Bangalore, India, 2010; pp. 1–5.
40. Dortch, J.M.; Owen, L.A.; Caffee, M.W.; Kamp, U. Catastrophic Partial Drainage of Pangong Tso, Northern India and Tibet. *Geomorphology* **2011**, *125*, 109–121. [CrossRef]
41. Huntington, E. Pangong: A Glacial Lake in the Tibetan Plateau. *J. Geol.* **1906**, *14*, 599–617. [CrossRef]

42. Rathour, R.; Gupta, J.; Mishra, A.; Rajeev, A.C.; Dupont, C.L.; Thakur, I.S. A Comparative Metagenomic Study Reveals Microbial Diversity and Their Role in the Biogeochemical Cycling of Pangong Lake. *Sci. Total Environ.* **2020**, *731*, 139074. [CrossRef] [PubMed]
43. Dvorský, M.; Klimeš, L.; Doležal, J. *A Field Guide to the Flora of Ladakh*, 1st ed.; Academia: Praha, Czech Republic, 2018; ISBN 978-80-200-2826-6.
44. Dvorský, M.; Altman, J.; Kopecký, M.; Chlumská, Z.; Řeháková, K.; Janatková, K.; Doležal, J. Vascular Plants at Extreme Elevations in Eastern Ladakh, Northwest Himalayas. *Plant Ecol. Divers.* **2015**, *8*, 571–584. [CrossRef]
45. Rawat, G.S. The Himalayan Vegetation along Horizontal and Vertical Gradients. In *Bird Migration across the Himalayas: Wetland Functioning amidst Mountains and Glaciers*; Prins, H.H.T., Namgail, T., Eds.; Cambridge University Press: Cambridge, UK, 2017; pp. 189–204. ISBN 978-1-316-33542-0.
46. Humbert-Droz, B. Impacts of Tourism and Military Presence on Wetlands and Their Avifauna in the Himalayas. In *Bird Migration across the Himalayas: Wetland Functioning amidst Mountains and Glaciers*; Prins, H.H.T., Namgail, T., Eds.; Cambridge University Press: Cambridge, UK, 2017; pp. 342–358. ISBN 978-1-316-33542-0. [CrossRef]
47. Ladon, P.; Nüsser, M.; Garkoti, S.C. Mountain Agropastoralism: Traditional Practices, Institutions and Pressures in the Indian Trans-Himalaya of Ladakh. *Pastoralism* **2023**, *13*, 30. [CrossRef]
48. Shaoliang, Y.; Ning, W.; Peng, L.; Qian, W.; Fusun, S.; Geng, S.; Jianzhong, M. Changes in Livestock Migration Patterns in a Tibetan-Style Agropastoral System: A Study in the Three-Parallel-Rivers Region of Yunnan, China. *Mt. Res. Dev.* **2007**, *27*, 138–145. [CrossRef]
49. Singh, R.; Sharma, R.K.; Babu, S. Pastoralism in Transition: Livestock Abundance and Herd Composition in Spiti, Trans-Himalaya. *Hum. Ecol.* **2015**, *43*, 799–810. [CrossRef]
50. Baghel, R.; Nüsser, M. Securing the Heights: The Vertical Dimension of the Siachen Conflict between India and Pakistan in the Eastern Karakoram. *Polit. Geogr.* **2015**, *48*, 24–36. [CrossRef]
51. Ghosal, S.; Ahmed, M. Pastoralism and Wetland Resources in Ladakh's Changthang Plateau. In *Bird Migration across the Himalayas: Wetland Functioning amidst Mountains and Glaciers*; Prins, H.H.T., Namgail, T., Eds.; Cambridge University Press: Cambridge, UK, 2017; pp. 333–341. ISBN 978-1-316-33542-0.
52. Namgail, T.; Bhatnagar, Y.V.; Mishra, C.; Bagchi, S. Pastoral Nomads of the Indian Changthang: Production System, Landuse and Socioeconomic Changes. *Hum. Ecol.* **2007**, *35*, 497–504. [CrossRef]
53. Qi, W.; Zhang, B.; Yao, Y.; Zhao, F.; Zhang, S.; He, W. A Topographical Model for Precipitation Pattern in the Tibetan Plateau. *J. Mt. Sci.* **2016**, *13*, 763–773. [CrossRef]
54. Böhner, J. General Climatic Controls and Topoclimatic Variations in Central and High Asia. *Boreas* **2006**, *35*, 279–295. [CrossRef]
55. Zhang, H.; Zhang, F.; Ye, M.; Che, T.; Zhang, G. Estimating Daily Air Temperatures over the Tibetan Plateau by Dynamically Integrating MODIS LST Data. *J. Geophys. Res. Atmos.* **2016**, *121*, 11425–11441. [CrossRef]
56. Xu, Z.X.; Gong, T.L.; Li, J.Y. Decadal Trend of Climate in the Tibetan Plateau—Regional Temperature and Precipitation. *Hydrol. Process.* **2008**, *22*, 3056–3065. [CrossRef]
57. Wang, X.; Pang, G.; Yang, M. Precipitation over the Tibetan Plateau during Recent Decades: A Review Based on Observations and Simulations. *Int. J. Climatol.* **2018**, *38*, 1116–1131. [CrossRef]
58. Schmidt, S.; Nüsser, M. Changes of High Altitude Glaciers in the Trans-Himalaya of Ladakh over the Past Five Decades (1969–2016). *Geosciences* **2017**, *7*, 27. [CrossRef]
59. Soheb, M.; Ramanathan, A.; Bhardwaj, A.; Coleman, M.; Rea, B.; Spagnolo, M.; Singh, S.; Sam, L. Multitemporal Glacier Inventory Revealing Four Decades of Glacier Changes in the Ladakh Region. *Earth Syst. Sci. Data* **2022**, *14*, 4171–4185. [CrossRef]
60. Dortch, J.M. Timing and Climatic Drivers for Glaciation across Semi-Arid Western Himalayan-Tibetan Orogen. *Quat. Sci. Rev.* **2013**, *78*, 188–208. [CrossRef]
61. Godwin-Austen, H.H. Notes on the Pangong Lake District of Ladakh, from a Journal Made during a Survey in 1863. *J. R. Geogr. Soc. Lond.* **1867**, *37*, 343–363. [CrossRef]
62. Lehner, B.; Verdin, K.; Jarvis, A. New Global Hydrography Derived from Spaceborne Elevation Data. *Eos Trans. Am. Geophys. Union* **2008**, *89*, 93. [CrossRef]
63. Crites, H.; Kokelj, S.V.; Lacelle, D. Icings and Groundwater Conditions in Permafrost Catchments of Northwestern Canada. *Sci. Rep.* **2020**, *10*, 3283. [CrossRef]
64. Schmidt, S.; Nüsser, M. Changes of High Altitude Glaciers from 1969 to 2010 in the Trans-Himalayan Kang Yatze Massif, Ladakh, Northwest India. *Arct. Antarct. Alp. Res.* **2012**, *44*, 107–121. [CrossRef]
65. Paul, F.; Huggel, C.; Kääb, A. Combining Satellite Multispectral Image Data and a Digital Elevation Model for Mapping Debris-Covered Glaciers. *Remote Sens. Environ.* **2004**, *89*, 510–518. [CrossRef]
66. Nüsser, M.; Schmidt, S. Glacier Changes on the Nanga Parbat 1856–2020: A Multi-Source Retrospective Analysis. *Sci. Total Environ.* **2021**, *785*, 147321. [CrossRef] [PubMed]
67. Racoviteanu, A.; Williams, M.W. Decision Tree and Texture Analysis for Mapping Debris-Covered Glaciers in the Kangchenjunga Area, Eastern Himalaya. *Remote Sens.* **2012**, *4*, 3078–3109. [CrossRef]
68. McFeeters, S.K. The Use of the Normalized Difference Water Index (NDWI) in the Delineation of Open Water Features. *Int. J. Remote Sens.* **1996**, *17*, 1425–1432. [CrossRef]

69. Hall, D.K.; Riggs, G.A.; Salomonson, V.V. Development of Methods for Mapping Global Snow Cover Using Moderate Resolution Imaging Spectroradiometer Data. *Remote Sens. Environ.* **1995**, *54*, 127–140. [CrossRef]
70. Walther, M.; Batsaikhan, V.; Dashtseren, A.; Jambaljav, Y.; Temujin, K.; Ulanbayar, G.; Kamp, U. The Formation of Aufeis and Its Impact on Infrastructure around Ulaanbaatar, North-Central Mongolia. *Erforsch. Biol. Ressourcen Mong.* **2021**, *14*, 385–398.
71. Huryn, A.D.; Gooseff, M.N.; Hendrickson, P.J.; Briggs, M.A.; Tape, K.D.; Terry, N.C. Aufeis Fields as Novel Groundwater-Dependent Ecosystems in the Arctic Cryosphere. *Limnol. Oceanogr.* **2021**, *66*, 607–624. [CrossRef]
72. Nüsser, M.; Schmidt, S.; Dame, J. Irrigation and Development in the Upper Indus Basin: Characteristics and Recent Changes of a Socio-Hydrological System in Central Ladakh, India. *Mt. Res. Dev.* **2012**, *32*, 51–61. [CrossRef]
73. Alekseev, V.R. Cryogenesis and Geodynamics of Icing Valleys. *Geodyn. Tectonophys.* **2015**, *6*, 171–224. [CrossRef]
74. Harden, D.; Barnes, P.; Reimnitz, E. Distribution and Character of Naleds in Northeastern Alaska. *Arctic* **1977**, *30*, 1–30. [CrossRef]
75. Wohl, E.; Scamardo, J.E. Aufeis as a Major Forcing Mechanism for Channel Avulsion and Implications of Warming Climate. *Geophys. Res. Lett.* **2022**, *49*, e2022GL100246. [CrossRef]
76. Kane, D.L. Physical Mechanics of Aufeis Growth. *Can. J. Civ. Eng.* **1981**, *8*, 186–195. [CrossRef]
77. Liu, W.; Fortier, R.; Molson, J.; Lemieux, J.-M. A Conceptual Model for Talik Dynamics and Icing Formation in a River Floodplain in the Continuous Permafrost Zone at Salluit, Nunavik (Quebec), Canada. *Permafr. Periglac. Process.* **2021**, *32*, 468–483. [CrossRef]
78. Terry, N.; Grunewald, E.; Briggs, M.; Gooseff, M.; Huryn, A.D.; Kass, M.A.; Tape, K.D.; Hendrickson, P.; Lane, J.W., Jr. Seasonal Subsurface Thaw Dynamics of an Aufeis Feature Inferred from Geophysical Methods. *J. Geophys. Res. Earth Surf.* **2020**, *125*, e2019JF005345. [CrossRef]
79. Pavelsky, T.M.; Zarnetske, J.P. Rapid Decline in River Icings Detected in Arctic Alaska: Implications for a Changing Hydrologic Cycle and River Ecosystems. *Geophys. Res. Lett.* **2017**, *44*, 3228–3235. [CrossRef]

Disclaimer/Publisher's Note: The statements, opinions and data contained in all publications are solely those of the individual author(s) and contributor(s) and not of MDPI and/or the editor(s). MDPI and/or the editor(s) disclaim responsibility for any injury to people or property resulting from any ideas, methods, instructions or products referred to in the content.